Thermostabilization Mechanism of Bovine Serum Albumin by Trehalose

ARTICLE *in* THE JOURNAL OF PHYSICAL CHEMISTRY B · MAY 2009

Impact Factor: 3.3 · DOI: 10.1021/jp900330r · Source: PubMed

Thermostabilization Mechanism of Bovine Serum Albumin by Trehalose

Alain Hédoux,* Jean-François Willart, Laurent Paccou, Yannick Guinet, Frédéric Affouard, Adrien Lerbret, and Marc Descamps

Laboratoire de Dynamique et Structure des Matériaux Moléculaires, UMR CNRS 8024, UFR de Physique, Université de Lille 1, Bat. P5, 59 655 Villeneuve d'Ascq Cedex, France

Received: January 13, 2009; Revised Manuscript Received: March 05, 2009

Thermal denaturation of bovine serum albumin (BSA) is analyzed from differential scanning calorimetry (DSC) and Raman spectroscopy investigations. DSC curves exhibit a marked dependence on protein concentration. BSA thermal denaturation becomes broader and bimodal, and the temperature of denaturation increases with increasing protein concentration. Raman scattering investigations simultaneously carried out in the low-frequency range (10−350 cm^{-1}) and in the amide I band region (1500−1800 cm^{-1}) indicate that the denaturation process is described as a biphasic process independent of protein concentration. The dependence of the protein stability upon the protein concentration can be interpreted from the coupling of protein and solvent dynamics. The confrontation of previous results obtained from Raman investigations on lysozyme (LYS) and the present study of BSA brings out significant information on protein dynamics and the coupling of protein and hydration-water dynamics in relation with the solvent accessible surface area. Contrary to LYS, the modification of the dynamics of hydration water by the protein is clearly observed on BSA. The influence of trehalose on the protein dynamics was analyzed. We found that trehalose reduces the dynamic fluctuations of polar side chains at the protein−solvent interface. The mechanism of thermostabilization by trehalose is related to the reduction of the exposure of hydrophobic groups of BSA to the water molecules, and to a strengthening of intermolecular O−H interactions in the hydrogen-bond network of water, leading to the stabilization of the tertiary structure.

I. Introduction

A considerable number of therapeutically highly promising biomolecules has become available due to the significant advances in recombinant DNA technology. However, their use is limited by their propensity to chemical and physical degradation. Controlling these degradations and improving the stability of biomolecules is thus one of the principal goals of the pharmaceutical industry today. Among disaccharides, considerable attention has been focused on trehalose because of its exceptional ability to protect biological materials under extreme conditions.[1−3] Several hypotheses have been proposed to explain the efficiency of trehalose. Some of them involve direct biomolecule−sugar−water interactions (water replacement model,[4] preferential hydration hypothesis[5]) or specific properties of sugar−water solutions such as the vitrification of solutions[6] or the influence of sugars on the water tetrahedral hydrogen-bond network.[7] However, the molecular mechanisms by which trehalose stabilizes proteins remain poorly understood and are sill debated on the basis of mentioned hypotheses, probably because the mechanisms are strongly dependent on the nature of applied stresses.

Combining Raman investigations in the 10−250 cm^{-1} low-frequency range and in the amide I band region (1500−1800 cm^{-1}) led to the description of lysozyme thermal denaturation as a two-step process.[8] The analysis of the low-frequency Raman spectrum has revealed a transformation of the tertiary structure between 65 and 75 °C in a highly flexible structure with intact secondary structure (first stage of thermal denaturation). This high flexibility favors the solvent penetration in the protein interior observed via an enhancement of the isotopic exchange corresponding to a frequency shift of the amide I band. The penetration of the solvent in the highly flexible tertiary structure is probably responsible for the breaking of the subtle balance between hydrophobic and hydrophilic interactions, leading to the unfolding process (second stage of thermal denaturation observed between 78 and 83 °C). It was observed that addition of sugars stabilizes the native tertiary structure, and limits the solvent penetration in the protein interior.[9] It was found that trehalose is a more efficient stabilizer of the tertiary structure with regard to other disaccharides (sucrose, maltose) because of its capability to distort the tetra-bonded H-bond network of water and to strengthen intermolecular O−H interactions responsible for the stability of the tertiary structure of lysozyme.

The structural organization of the H-bond network of the solvent both in the hydration shell and in the bulk (i.e., near and far from the protein surface) is closely involved in the protein stability. This structural organization is dependent on the nature of the solvent and probably on the structural properties of the protein.

To give a better description of the mechanisms by which sugars thermostabilize proteins, and to explain the exceptional properties of trehalose, it is necessary to analyze sugar-induced thermostabilization of different proteins. Lysozyme (LYS, 14.3 kDa) is a globular protein with relatively strong internal cohesion, mainly composed of α-helices.[10] Bovine serum albumin (BSA) is also a globular protein mainly composed of α-helices. By contrast to LYS, BSA has a higher molecular weight (66 kDa) than LYS and is well-known for its conformational adaptability. Significant differences in the solvent-accessible surface area (SASA) between LYS and BSA can be expected from the consideration of their molecular weight. 193L[11] entry of the Protein Data Bank was used to compute

* Corresponding author.

10.1021/jp900330r CCC: $40.75
Published on Web 04/01/2009

SASA of the crystalline structure of lysozyme. A value of about 7000 Å[212] was obtained by using the program DSSP.[13] Since the structure of bovine serum albumin is still unknown, 1UOR[14] corresponding to human serum albumin and expected to be very similar to BSA was used to calculate the SASA of BSA to about 30 000 Å^2. It is recognized that SASA is directly connected to the protein stability, and it is previously reported that trehalose could stabilize proteins by making unfavorable the increase of SASA[3,12] in the framework of the preferential hydration hypothesis.[15] Consequently, it is expected that the confrontation of investigations in BSA and LYS reveals additional information on the mechanism of protein stabilization, in relation to their structural and dynamical properties.

In a first stage, BSA thermal denaturation is analyzed by calorimetry and microcalorimetry investigations, for BSA dissolved in H_2O with protein concentrations in the 0.5−5 mM/L range. DSC curves are interpreted from Raman investigations carried out both in the low-frequency range and in the amide I band region. This latter is a direct probe of the secondary structure, but can also be used to observe changes in the tertiary structure via the detection of a frequency shift connected to H−D isotopic exchanges.[8,16] In this context, Raman scattering experiments were mainly performed on BSA dissolved in D_2O (BSA/H_2O) at two protein concentrations: 1.7 and 5 mM/L.

In a second stage the influence of trehalose on the mechanism of BSA thermal denaturation is analyzed. Taking into account the difficulty to obtain homogeneous mixtures of BSA, D_2O, and trehalose, BSA, H_2O, and trehalose (BSA/H_2O/T40) ternary mixtures have been analyzed, corresponding to 40 wt % of trehalose in water and the protein concentration at 5 mM/L. Ternary mixtures BSA/D_2O/T40 have been analyzed at 1.7 mM/L protein concentration. The 40% sugar weighted concentration corresponds to a threshold concentration from which the influence of trehalose on the H-bond network of water can be distinguished from that of other disaccharides.[17,18]

II. Materials and Methods

Samples. Bovine serum albumin (BSA, 66 kDa) was purchased from Sigma as lyophilized powder (purity minimum 98%). High-purity trehalose dihydrate was supplied from Fluka and Sigma. First, the trehalose water mixtures (H_2O/T40) were prepared at the desired concentration (40 wt % trehalose) and thereafter the protein was added. Ternary solutions with 40 mass % trehalose concentration was systematically used. The protein-containing mixtures were agitated in an Eppendorf agitator at about 298 K with about 1000 turns/min. Trehalose/water weight proportions were prepared using double-distilled pure water. The protein concentrations 0.5, 1, 1.5, 3.4, and 5 mM/L are used. This latter ensures about 10 hydration shells surrounding the protein molecules in water that limits the direct protein−protein interactions. The mixtures were loaded in hermetically closed 10 × 5 mm quartz cuvettes. Measurements were carried out in the 295−380 K temperature range on samples at pH 6.8.

Modulated-temperature differential scanning calorimetry (MDSC) was performed using the MDSC 2920 microcalorimeter of TA Instruments. The temperature and enthalpy readings were calibrated using pure indium. Only heating runs were performed with a scanning rate of 1 °C/min. Sample mass was 13.80 and 11.73 mg, respectively, for BSA/H_2O and BSA/H_2O/T40 mixtures. In order to analyze the thermodynamic features of the first-order transition associated to the thermal denaturation, suitable modulation parameters were found to be 100 s for the period of modulation and 0.212° for the modulation amplitude. The C_p reading was calibrated using a standard sapphire sample in the temperature range of study. The enthalpy of denaturation was determined by integration of the heat flow trace using the sigmoidal tangents above and below the denaturation peak as a baseline. The C_p jump (ΔC_p) resulting from the denaturation was determined from the difference in the C_p curve on both sides of the endothermic peak, using the TA software.

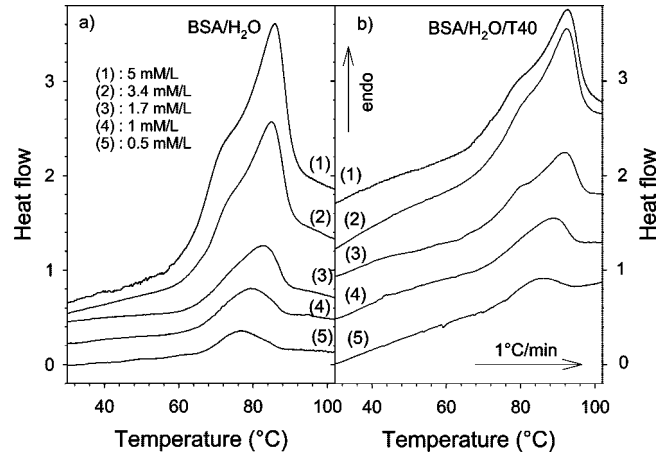

Figure 1. DSC curves as a function of protein concentration for BSA/H_2O solutions (a) and BSA/H_2O/T40 solutions (b) obtained by microcalorimetry measurements.

DSC was also carried out on a very sensitive microcalorimeter (microDSC III, Setaram). Typical sample mass of 400 mg was used for BSA/H_2O and BSA/H_2O/T40 mixtures. Only heating runs were performed with a scanning rate of 1 °C/min. The enthalpy of denaturation was determined using Setaram software, by integration of the heat flow after subtraction of the sigmoidal baseline tangent to the heat flow trace above and below the endotherm of denaturation.

Raman spectroscopy was performed using a XY Dilor spectrometer with a 514.5 nm Ar−Kr laser and 20 mW of incident power. Spectra were recorded in the 10−300 cm^{-1} range and in the 1500−1800 cm^{-1} range (amide I band region) by measuring in backscattering geometry. The mixtures were loaded in Hellma quartz-Suprasil cells and hermetically sealed. A fluorescence contribution to the spectra appeared systematically in the background signal. Its magnitude was approximated by a second-order polynomial using a fitting procedure, and then subtracted from the spectra.

III. Results

A. Thermodynamic Analysis. Due to its high sensivity, microcalorimetry gives the opportunity to analyze thermal denaturation on hydrated BSA for low protein concentrations. Measurements are first carried out for both BSA dissolved in H_2O (BSA/H_2O) and in H_2O/trehalose (BSA/H_2O/T40) mixtures with protein concentrations within 0.5−5 mM/L. DSC traces are plotted in Figure 1, and the thermodynamic characteristics of the thermal denaturation, i.e., the melting temperature (T_m, temperature at which a maximum occurred in the endothermic peak) and the enthalpy of thermal denaturation (ΔH), are determined using Setaram software and reported in Tables 1 and 2.

A first set of experiments concerning (BSA/H_2O) samples is reported in Figure 1a. It reveals that the endothermic peak clearly exhibits a dependence upon concentration. Figure 1a and Table 1 indicate that the protein stability decreases with decreasing protein concentration. Protein concentration has also an influence on the shape of the denaturation endotherm. Protein thermal denaturation is monophasic for low concentration, as reflected

TABLE 1: Thermodynamic Parameters of Thermal Denaturation of BSA Dissolved in H_2O from Microcalorimetry Experiments

	0.5 mM/L	1 mM/L	1.7 mM/L	3.4 mM/L	5 mM/L
T_m (°C)	75.7 ± 0.1	78.6 ± 0.1	81.9 ± 0.1	84.9 ± 0.1	85.3 ± 0.1
ΔH (kJ/mol)	990 ± 50	960 ± 40	1080 ± 40	977 ± 30	1050 ± 20

TABLE 2: Thermodynamic Parameters of Thermal Denaturation of BSA Dissolved in H_2O/T40 from Microcalorimetry Experiments

	0.5 mM/L	1 mM/L	1.7 mM/L	3.4 mM/L	5 mM/L
T_m (°C)	84.8 ± 0.1	87.4 ± 0.1	91.4 ± 0.1	92.2 ± 0.1	92.7 ± 0.1
ΔH (kJ/mol)	1084 ± 50	956 ± 40	1110 ± 50	962 ± 30	985 ± 20

TABLE 3: Thermodynamic Parameters on BSA Thermal Denaturation Dissolved in H_2O and H_2O/T40 at BSA Concentration 5 mM/L, from DSC and MDSC Experiments[a]

	T_m(DSC) (°C)	T_m(MDSC) (°C)	ΔH(DSC) (kJ/mol)	ΔH(MDSC) (kJ/mol)	ΔC_p(MDSC) kJ/(mol °C)
BSA/H_2O	85.3 ± 0.1	83.8 ± 0.1	1050 ± 20	1159 ± 30	34 ± 5
BSA/H_2O/T40	92.7 ± 0.1	91.5 ± 0.1	985 ± 20	1170 ± 30	34 ± 5
LYS/H_2O	–	73.3± 0.1	–	386 ± 11	4.3 ± 0.5
LYS/H_2O/T40	–	83.7 ± 0.1		450 ± 10	3.6 ± 0.5

[a] Data on LYS are obtained from ref 2.

by a single endotherm. The endothermic peak becomes broader and dissymmetric with increasing protein concentration. Above 1.7 mM/L BSA, thermal denaturation is described by two overlapping endothermic peaks. This first set of measurements points out a decrease in stability of BSA with increase in water concentration, whereas the enthalpy of the protein denaturation is nearly independent of the concentration. This result is consistent with a previous analysis of Michnik et al.[19] performed on BSA solutions corresponding to protein concentrations of 0.022 and 0.044 mM/L. For these very low concentrations, only one endothermic peak was detected by microcalorimetry measurements. Moreover, BSA was observed to denature at T_m = 66 °C in solution at pH 7, for 0.044 mM/L BSA concentration, which is consistent with results reported in Table 1. However, the decrease in stability of defatted human albumin (HSA) with increase in protein concentration has been reported[20] from calorimetric investigations. This phenomenon was interpreted from the consideration that polymerization of denatured monomer promotes unfolding.[20]

A second set of DSC measurements was carried out on BSA/H_2O/T40 solutions with protein concentration in the 0.5−5 mM/L range by microcalorimetry (Figure 1b). They clearly reveal an increase of the protein stability in presence of trehalose. From Figure 1b and Table 2, it is clearly observed that BSA denatures at higher temperature in the presence of trehalose, whereas the enthalpy of denaturation remains nearly unchanged. It can be observed that BSA thermal denaturation in solution (1.7 mM/L) becomes clearly biphasic in presence of trehalose whereas the endotherm was merely dissymmetric in BSA/H_2O solution. From both set of experiments (with and without trehalose), it can be observed that the tendency for biphasic thermal denaturation is more pronounced for increasing stability.

MDSC experiments were performed for solutions with 5 mM/L protein concentration corresponding to the limit of sensitivity of the technique providing reliable data. This study was also performed in the presence of trehalose. MDSC measurements give the opportunity to provide additional C_p traces (Figure 2). From these C_p traces, the C_p jumps (ΔC_p) accompanying the denaturation are determined and reported in Table 3.

Both MDSC and DSC experiments carried out on high-concentration solutions (5 mM/L) are converging into a bimodal description of BSA thermal denaturation.

MDSC experiments reveal that the C_p jump is spreading out over a wide temperature range (~30 °C) roughly corresponding to the first endothermic peak.

BSA dissolved in D_2O (BSA/D_2O, 5 mM/L) was analyzed by microcalorimetry, since Raman data are mainly obtained on BSA/D_2O samples. DSC traces have the same shape as for BSA/H_2O and reflected a biphasic denaturation and were not plotted in this paper. Only the thermodynamic data are reported in Table 3. As expected from previous studies on BSA[21] and lysozyme,[8,21] BSA denatures at higher temperatures than that dissolved in H_2O.

B. Raman Spectroscopy. ***1. Analysis of the Amide I Band Region (1500−1800 cm^{-1}).*** The analysis of the amide I band region provides the opportunity to monitor the secondary structure of proteins. The Raman spectrum in the 1500−1800 cm^{-1} region is plotted in Figure 3 for the native and denatured states of BSA dissolved in D_2O and in D_2O/T40 for 1.7 mM/L protein concentration. It is dominated by a broad Raman band near 1646 cm^{-1} corresponding to the C═O stretching vibration of amide groups coupled to the in-phase bending of the N−H bond and the stretching of the C−N bond.[22] The Raman band observed near 1610 cm^{-1} (localized by an arrow in Figure 3)

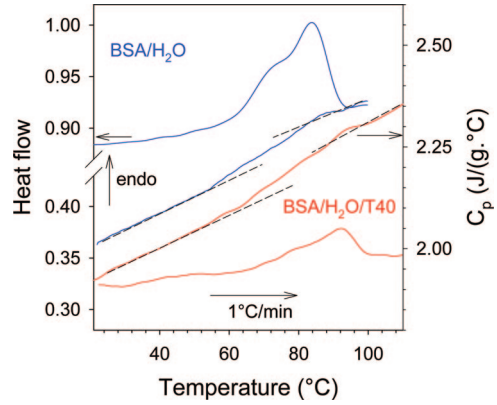

Figure 2. Heat flow and C_p traces obtained by MDSC experiments on BSA/H_2O and BSA/H_2O/T40 solutions.

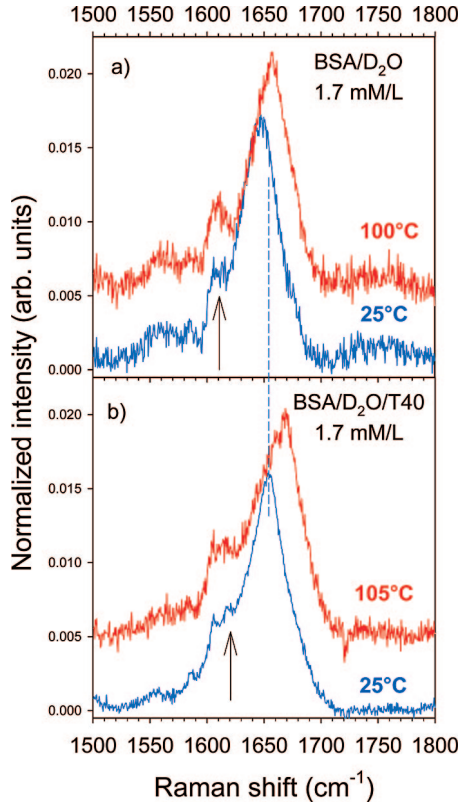

Figure 3. Raman spectrum in the amide I band region in the native and denatured states for (a) BSA/D_2O solution and (b) BSA/D_2O/T40 solution at BSA concentration 1.7 mM/L. For better clarity, the spectra of the native and denatured states are arbitrarily shifted along the intensity axis. The arrow localizes the band which probes the molecular aggregation.

was assigned to the intermolecular β-sheet interactions and can be used to probe molecular aggregation via the increase of its intensity.[16,23] Figure 3 clearly indicates that no aggregation was detected in experiments carried out on hydrated BSA and on BSA/D_2O/T40 solutions. The extreme similarity between the Raman spectra of the amide I band of BSA in the presence (Figure 3b) or absence (Figure 3a) of trehalose indicates a similar secondary structure in a water or in a sugar environment according to previous studies.[2,24]

The Raman spectrum of proteins in the region of the amide I band results from the overlapping of Raman bands corresponding to different kinds of vibrations and to different molecular conformations. The amide I band was analyzed by a global analysis method, in which the different contributions to the amide I band were described as a Gaussian line shape. The temperature dependence of the amide I band frequency is plotted for BSA dissolved in D_2O (Figure 4a) and BSA dissolved in H_2O/T40 (Figure 4b). As expected, Figure 4 first indicates a downshift of the amide I band frequency, at room temperature, in BSA/D_2O solutions with respect to that determined in BSA/H_2O mixtures. This frequency shift is explained by isotopic exchanges NH/ND according to previous studies on proteins dissolved in D_2O.[8,22] Figure 3 indicates that isotopic exchanges are limited in presence of trehalose, since the dashed line clearly shows that the frequency of the amide I band in BSA/D_2O/T40 is higher than in BSA/D_2O at room temperature. It is the consequence of the reduction of isotopic exchanges between D_2O and BSA which could be inherent from the combination of different phenomena: (i) a reduction of the solvent mobility near the surface of BSA, (ii) isotopic exchanges between D_2O and trehalose, and (iii) interactions between trehalose and BSA. This feature could be connected to a reduction of the SASA in presence of trehalose. By temperature increase, an additional shift is clearly observed above 40 °C for a 5 mM/L protein concentration. Similar additional H−D exchanges have been previously observed in different proteins[8,16,23] and interpreted as the result of a change in the tertiary structure leading to enhanced solvent accessibility. This latter corresponds to the exposition to the solvent of protein core characterized by residues with low solvent accessibility in the native tertiary structure. It is worth noting that the enhancement of the isotopic H−D exchange and thus the solvent penetration in BSA is almost undetectable for the 1.7 mM/L BSA/D_2O solution. Consequently, the presence of trehalose can be considered as limiting the exposure of hydrophobic groups, as previously observed in lysozyme,[9] and then stabilizing the tertiary structure. The mechanism of protein stabilization by trehalose can be described as the limitation of the protein hydration by making unfavorable the increase of the solvent accessible surface area of proteins upon denaturation, as previously reported.[3,9,25]

Temperature dependences of the amide I band frequency are fitted by a least-squares refinement method using the equation $\nu = [(\nu_N - \nu_D)/(1 + \exp((T - T_m)/\Delta T))] + \nu_D$, where T_m is the transition midpoint temperature, $2 \times \Delta T$ corresponds to the temperature domain of the transition, and ν_N and ν_D are the frequencies of the amide band in the native and denatured states, respectively. The values (T_m, ΔT) determined by the fitting procedures are reported in Table 4. A good agreement is observed between Raman and calorimetric data. It is worth to notice that the unfolding process analyzed through the frequency shift of the amide I band corresponds to the second endotherm for samples at high protein concentration.

Figure 4b shows that the unfolding curve is clearly shifted toward high temperatures in presence of trehalose.

2. Analysis of the Low-frequency Raman Spectrum (10 cm^{-1}; 300 cm^{-1}). The scattered low-frequency intensity of amorphous materials is composed of a quasielastic component and harmonic vibrations which overlap in the 10−100 cm^{-1}. It was transformed into reduced intensity $I_r = I(\nu)/(\nu[n(\nu) + 1])$, where $n(\nu)$ is the Bose factor. The reduced intensity was transformed into Raman susceptibility ($\chi''(\nu) = \nu I_r(\nu)$) after subtraction of the quasielastic component usually associated to a Lorentzian line shape. The Raman susceptibility is recognized to be representative of the vibrational density of states (VDOS, $g(\nu)$) via the relation $\chi''(\nu) = C(\nu)g(\nu)/\nu$, where $C(\nu)$ is the light−vibration coupling coefficient.

The Raman susceptibility of pure D_2O and its modifications by addition of BSA are plotted in Figure 5a. The spectrum of pure D_2O is composed of two broad bands near 60 and 170 cm^{-1}. The assignment of these bands was performed from theoretical and experimental investigations performed on H_2O.[26] The low-frequency band is assigned to the translation of a water molecule, restricted by a cage composed of neighboring D_2O molecules, and this band is generally associated with the "cage" effect for any liquid. The Raman band observed around 170 cm^{-1} in D_2O can be assigned to the intermolecular O−D stretching within the hydrogen bond network. This stretching vibration is generally described as a restricted translation of the D_2O molecules in the O−D···O direction, whereas the 60 cm^{-1} band is associated with the restricted translation of D_2O molecules perpendicular to the O−D···O direction. It is clearly observed that the intensity of the low-frequency band increases with addition of BSA, to the detriment of that of the 170 cm^{-1} band, reflecting a structural modification of the H-bond network

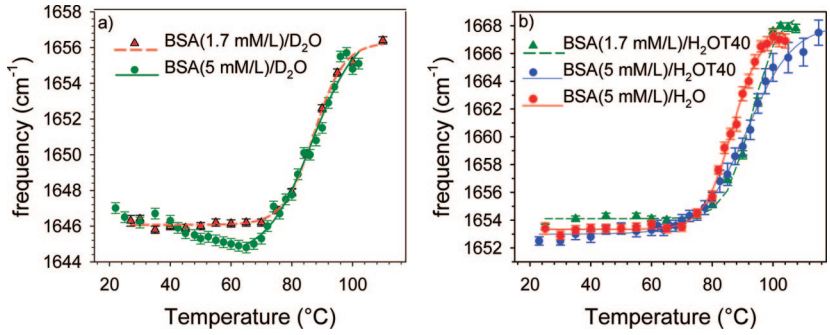

Figure 4. Temperature dependence of the amide I band frequency for (a) BSA dissolved in D_2O at two BSA concentrations, 1.7 and 5 mM/L; (b) BSA dissolved in H_2O (5 mM/L) and in H_2O/T40 (5 mM/L and 1.7 mM/L).

TABLE 4: Thermal Parameters of the Unfolding Process Obtained by the Fitting Procedure Defined in the Text[a]

	T_m (°C)	ΔT (°C)
BSA(1.7 mM/L)/D_2O	87.0 ± 0.4	4.5 ± 0.3
BSA(5 mM/L)/D_2O	86.9 ± 0.6	7.5 ± 1
BSA(5 mM/L)/H_2O	86.5 ± 0.3	4.5 ± 0.3
BSA(1.7 mM/L)/H_2OT40	93.0 ± 0.7	4.3 ± 0.5
BSA(5 mM/L)/H_2OT40	91.6 ± 0.5	7.5 ± 0.4

[a] The result of the fitting procedure is plotted in Figure 4.

of D_2O. A shift of the 60 cm^{-1} band toward high frequencies is also observed. This indicates that the cage is more rigid in the BSA/D_2O mixture than in D_2O. The high-frequency band peaking around 170 cm^{-1} in the spectrum of D_2O splits into two contributions localized by two arrows in the spectrum corresponding to the protein concentration of 5 mM/L. These two contributions have probably the same origin as the 170 cm^{-1} band in the spectrum of D_2O, i.e., the restricted translation of D_2O molecules in the O—D···O direction, but correspond to two different types of D_2O network. From consideration on their frequency, the low-frequency component peaking around 170 cm^{-1}, as observed in the spectrum of D_2O, should be assigned to the intermolecular O—D stretching in the bulk D_2O, whereas the component observed around 210 cm^{-1} could correspond to the same vibration in the hydration water, corresponding to a molecular association between BSA and D_2O via (O—D···O) hydrogen bonding. The Raman susceptibility of BSA/D2O is plotted for 1.7 and 5 mM/L protein concentrations in Figure 5b, corresponding respectively to a monophasic and biphasic denaturation process from DSC measurements carried out on BSA/H_2O mixtures (Figure 1a). In the spectrum of the mixture corresponding to the lower protein concentration, the 170 cm^{-1} component is mainly observed, whereas the 210 cm^{-1} contribution is clearly observed in the spectrum of the high protein concentration mixture (5 mM/L), at the expense of the 170 cm^{-1} band.

The Raman susceptibility of this mixture (5 mM/L of BSA in D_2O) is compared in Figure 5c with that of LYS/D_2O for a protein concentration of 14.6 mM/L obtained from a previous study. The two different protein concentrations correspond nearly to the same number (10) of hydration shells around the protein. The low-frequency component of the spectrum associated to the motions in the cage is roughly similar for BSA/D_2O and LYS/D_2O mixtures. The main difference between both spectra concerns the Raman band corresponding to the translational vibration of D_2O molecules in the O—D···O direction, which characterizes the structural organization in the solvent around the protein. Only one band is detected in the spectrum of LYS/D_2O, corresponding to the Raman bands observed in the spectra of D_2O and BSA/D_2O near 170 cm^{-1}, whereas an

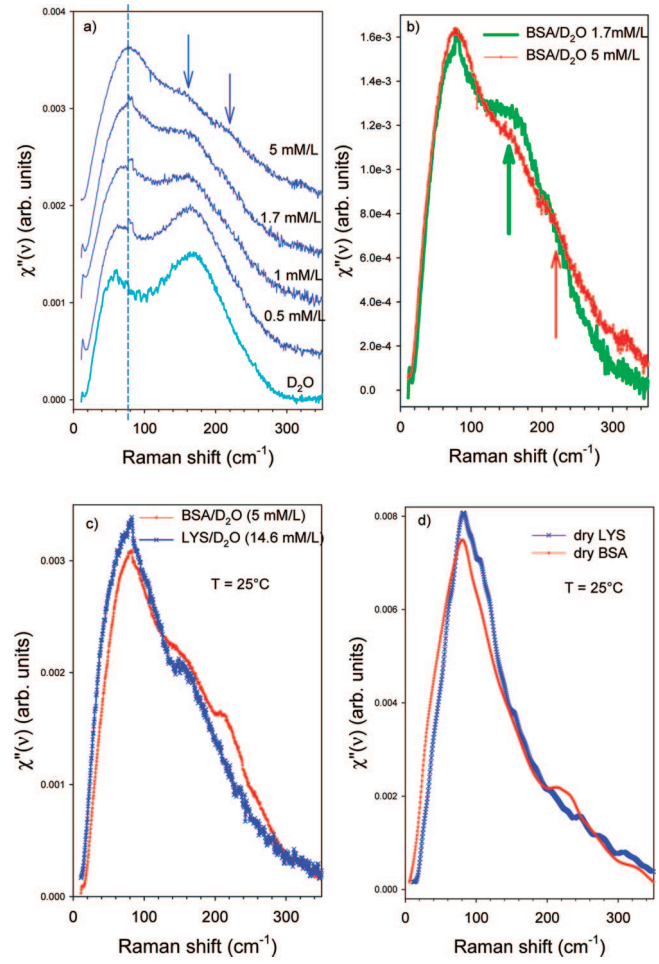

Figure 5. Representation of the Raman susceptibility of BSA (a) in solution with D_2O with different BSA concentrations, and compared with the spectrum of D_2O; (b) in solution with D_2O for 1.7 and 5 mM/L protein concentrations; the arrows localize both 170 and 210 cm^{-1} components of the intermolecular O—D stretching vibrations, respectively, in the bulk water and hydration water which are observed for the high protein concentration (5 mM/L); only the 170 cm^{-1} component is observed in the spectrum corresponding to the low protein concentration (1.7 mM/L); (c) in solution with D_2O (5 mM/L) compared with LYS in solution with D_2O (14.5 mM/L); (d) dry BSA powder compared with dry LYS.

additional component is observed near 210 cm^{-1} in the spectrum of BSA/D_2O. This component corresponds to a marked shoulder in the spectrum of dry BSA (Figure 5d) which is not detected in the spectrum of dry LYS. This shoulder observed near 210 cm^{-1} is probably corresponding to the vibrations of polar residues involved in the O—D···O intermolecular association with the hydration water, since it is located around the same

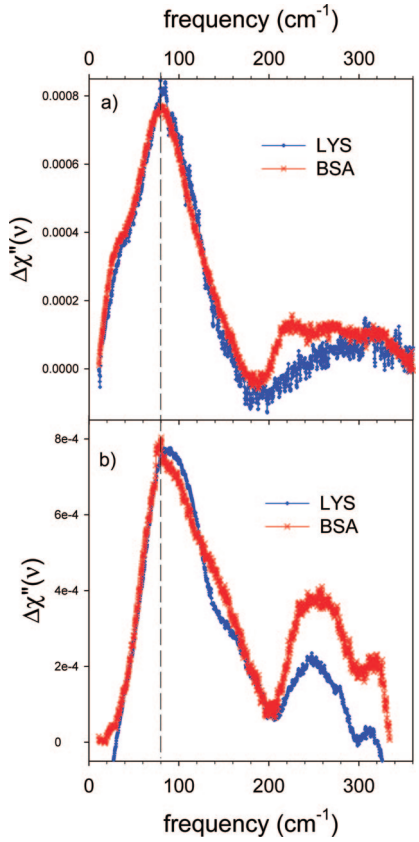

Figure 6. Comparison between the difference spectra $\Delta\chi''(\nu)$ of BSA and LYS representative of the BSA and LYS dynamics alone in the presence of (a) H_2O and (b) H_2O/T40.

frequency than the high-frequency component of the intermolecular O−D stretching in D_2O in the spectrum of BSA/D_2O (Figure 5a). This can be considered as the signature of a significant coupling between the polar side chains and the dynamics of the solvent at the BSA−D_2O interface. This assignment reflects that the protein does not drastically influence the dynamics of the water up to 1.7 mM/L protein concentration, whereas at 5 mM/L the signature of the coupling between the dynamics of BSA and the hydration water (near 210 cm^{-1}) is clearly observed. The comparison between the spectra of dry LYS and LYS/D_2O merely confirms the assignment of the 170 cm^{-1} band in the spectrum of LYS/D_2O as representative of the intermolecular O—D···O stretching in D_2O.

Information on the protein dynamics is expected from the analysis of $\Delta\chi''(\nu)$ spectrum (Figure 6a) where the contribution of the bulk water spectra is removed by subtracting the appropriate fraction (about 75%, corresponding to the relative proportion of D_2O in the mixture) of the bulk H_2O susceptibility from that of BSA/H_2O solution at 5 mM/L protein concentration. This transformation gives the opportunity to analyze mainly the dynamics of the protein alone in presence of water, despite of the contribution from hydration water. The $\Delta\chi''(\nu)$ spectrum of BSA is compared to that of LYS. The spectra are also composed of two broad bands. The broad band with maximum intensity at around 80−90 cm^{-1} appeared to be superimposed for both BSA and LYS proteins. It is assigned to motions of the protein backbone according to previous studies.[27,28]

The second broad band peaking around 280 cm^{-1} in the $\Delta\chi''(\nu)$ spectrum and spreading out between 200 and 350 cm^{-1} is detected in agreement with previous observations by ultrafast optical heterodyne-detected Raman-induced Kerr-effect spectroscopy[27] and Raman spectroscopy.[28] This frequency range between 200 and 350 cm^{-1} is characteristic of strong interactions similar to those observed in highly polar ionic liquids.[29] Consequently, this broad band can be considered as the signature of strong interactions between the polar side chains and the solvent via H-bonding, reflecting a strong coupling between the dynamics of BSA and H_2O. The observation of the tail in the high-frequency side of the intense band in the $\chi''(\nu)$ spectrum of dried powder BSA (Figure 5d) in the 200−350 cm^{-1} frequency range, where the broad high-frequency band is detected in the $\Delta\chi''(\nu)$ spectrum, suggests that polar side chains could interact with residual water in the dry state of BSA.

The main difference between the two $\Delta\chi''(\nu)$ spectra of BSA and LYS concerns the broad high-frequency band. The enhanced intensity observed in the $\Delta\chi''(\nu)$ spectrum of BSA between 200 and 300 cm^{-1}, with respect to that of LYS (Figure 6a), probably reflects additional vibrations of polar residues in BSA, and involved in H-bonding association to the solvent. This is consistent with the larger SASA of BSA compared to that of LYS.

The dynamics of BSA and LYS alone in water/trehalose solution can be also analyzed via the plot of $\Delta\chi''(\nu)$ spectra reported in Figure 6b, obtained by subtracting the susceptibility of the bulk H_2O/T40 from the susceptibility of the BSA/H_2O/T40 and LYS/H_2O/T40 ternary mixtures. The comparison of parts a and b of Figure 6 reveals significant information on the protein dynamics in the presence of trehalose. First, the low-frequency component of the $\Delta\chi''(\nu)$ spectra, assigned with the cage effect of the atoms of the protein backbone, is significantly shifted toward the high frequencies in the presence of trehalose. It can be outlined that the frequency of maximum intensity remains nearly constant for BSA, but the distribution of the BSA dynamic fluctuations is clearly centered at higher frequencies. Consequently, addition of trehalose induces a stiffening of the cage, in relation with an increase of the viscosity of the mixture. Some changes can be also detected in the line shape of this band around 20−40 cm^{-1} which could be inherent to changes in solvent−protein interactions and so to modifications in the SASA. Second, the high-frequency component becomes sharper and its intensity increases in the presence of trehalose, especially for BSA. The sharpening of this band corresponds to a decrease of the distribution of the solvent−protein interactions via H-bonds, and a concomitant reduction of the dynamic fluctuations of polar side chains at the solvent−protein interface. In the spectrum of BSA, the maximum intensity of this band is detected around 250 cm^{-1}, indicating a strengthening of solvent−protein interactions with respect to the component detected near 210 cm^{-1} in the $\Delta\chi''(\nu)$ spectrum of BSA in Figure 6a. Consequently, Figure 6a,b shows that the motions of surface atoms are more sensitive to the dynamics of the solvent than the core atoms, as previously determined from molecular-dynamics simulations on lysozyme.[30]

3. Temperature Dependence of the Raman Susceptibility of BSA/H_2O and BSA/H_2O/T40 Mixtures. The Raman susceptibilities of BSA dissolved in H_2O and H_2O/T40 at 5 mM/L are plotted in Figure 7 in the native (a) and denatured (b) states. Raman spectra were fitted using the residue method of the PeakFit software. The result of the fitting procedure of the Raman susceptibility of BSA/H_2O mixtures reveals that three Raman bands (localized by arrows in Figure 7a) are needed to obtain a satisfactory agreement between fitted and experimental data at room temperature, whereas the Raman susceptibility in the denatured state is only composed of two Raman bands (Figure 7b). As previously shown, in the native state (Figure 7a), component (1) corresponds to the cage effect, component

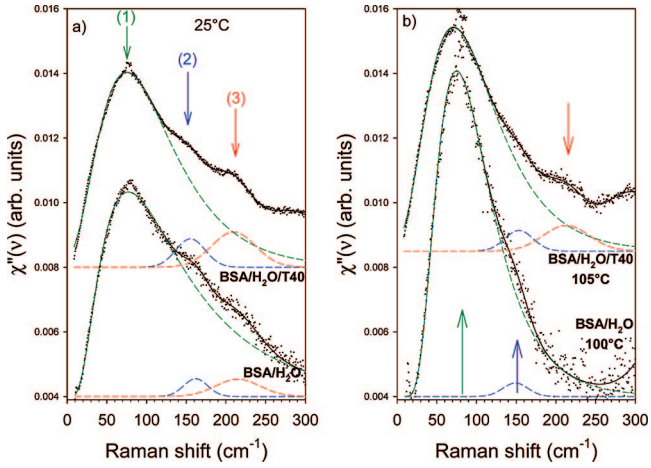

Figure 7. Raman susceptibility spectra of BSA dissolved in H_2O, in H_2O, and in H_2O/T40 in the native state at room temperature (a), and in the denatured state near 100 °C (b). Solid lines correspond to the result of a fitting procedure, and dashed lines to the components of the spectrum determined by the fitting procedure. The frequencies of these components are localized by arrows. The star localizes a laser line.

(2) to the intermolecular O−H stretching vibration in the bulk water, and component (3) to the same motion in the hydration water.

In the presence of trehalose, the $\chi''(\nu)$ spectrum of BSA/H_2O/T40 is not drastically modified after BSA thermal denaturation (Figure 7b) in opposition to BSA dissolved in H_2O. The transformation of the spectra of BSA/H_2O after denaturation shows the softening of intermolecular O−H interactions of water and a concomitant breaking of the H-bond network of water. Addition of trehalose strengthens the intermolecular O−H interactions in the H-bond network of water and then stabilizes the structural organization of the solvent in the bulk and in the hydration water, as observed in lysozyme.[2] The signature of the hydration water remains observed at 100 °C in the presence of trehalose and not without trehalose. This indicates that trehalose keeps the water hydration around the protein.

IV. Discussion

This work first reveals that the profiles of DSC curves show a marked dependence on protein concentration. The stability of BSA is clearly dependent on the concentration, and thermal denaturation can be described either as a monophasic or biphasic transformation depending on protein concentration. Increasing protein concentration up to 1.7 mM/L induces a tail on the low-temperature side of the endothermic peak of thermal denaturation, and a concomitant shift of T_m toward high temperatures. With further increase of protein concentration the transition becomes very broad and bimodal. This is the first observation of biphasic transition in bovine albumin in opposition to porcine, canine, and human albumin,[31] which could be related to the low degree of purity (98% minimum). In the present study, the first endothermic peak is associated with the transformation of the tertiary structure induced by structural modifications in the H-bond network of water by heating. This transformation is characterized by an enhanced exposition of hydrophobic residues to the solvent, observed via the downshift of the amide I band reflecting enhanced H−D isotopic exchanges. Water penetration in the protein interior destabilizes the tertiary structure of BSA as observed in the first stage of lysozyme thermal denaturation,[8] in agreement with previous calorimetric studies,[32] despite the observation of only one endothermic peak. The description of the protein thermal denaturation as a biphasic process should be a general feature for globular proteins, and the observation of endotherms with two distinct peaks could be inherent to the transformation of the tertiary structure (first step of denaturation) over a wide temperature range. Figure 2 clearly shows that the C_p jump is associated with the low-temperature endothermic peak, corresponding to the transformation of tertiary structure with intact secondary structure. Consequently, the C_p jump which is generally observed during the thermal denaturation should be mainly distinctive of the change of the flexibility of the protein tertiary structure and to the enhanced exposition of hydrophobic residues to the solvent, as previously observed in LYS.[8]

The confrontation of the Raman investigations on BSA to those performed on lysozyme provides information about the influence of the SASA on the dynamical properties of the protein in relation with the protein stability. The high molecular weight of BSA compared with that of LYS generates significant difference between SASA of the two proteins (30 000 Å^2 for BSA and 7000 Å^2 for LYS).

The difference between SASA of BSA and LYS is observed via the analysis of the amide I band at room temperature. For protein/D_2O mixtures, the frequency of this band is shifted toward low frequencies with respect to that in protein/H_2O mixtures, because of H−D isotopic exchanges between solvent and protein at the protein−solvent interface. At room temperature, the downshift in BSA is about 7 cm^{-1} (instead of 3 cm^{-1} in lysozyme). A larger frequency shift is consistent with a larger protein surface accessible to the solvent. The SASA has probably an influence on the first step of the thermal denaturation, since the enhanced isotopic exchange (associated with this first step of denaturation) is detected in BSA between 40 and 70 °C and corresponds to a downshift of about 2 cm^{-1}, while in lysozyme a downshift of about 5 cm^{-1} is detected in a narrower temperature range (60−70 °C). This feature reflects a lower stability of the tertiary structure of BSA than that of lysozyme, which could be a direct consequence of the structural organization and the dynamical properties of the solvent at the water−protein interface.

The analysis of the low-frequency Raman spectrum provides significant information on the dynamics of the protein and the solvent. This study reveals that the main difference between the dynamics of BSA and LYS in water concerns the vibration of the polar residues involved in molecular association with water via H-bonding, whereas the dynamics of the core of both proteins is very similar. The spectra of BSA/D_2O and LYS/D_2O mixtures (Figure 5c) are mainly distinguishable in the frequency range 130−290 cm^{-1} where intermolecular O−D stretching vibrations in the hydrogen bond network of the solvent are observed. This is probably the signature of a stronger coupling between the dynamics of the BSA and the solvent, induced by a larger SASA, which makes the distinction between bulk water and hydration water observable. Consequently, BSA modifies the structure and the dynamics of hydration water in a larger extent than LYS, since no distinction can be detected between bulk and hydration water, from the analysis of the low-frequency spectrum of hydrated lysozyme (Figure 5c). This feature is connected with the observation of the enhanced intensity in the $\Delta\chi''(\nu)$ spectrum of BSA above 200 cm^{-1} (Figure 6a), reflecting additional vibrations of polar residues in BSA with respect to lysozyme. The concentration dependence of the BSA stability can be related to the extent of the coupling between the dynamics of BSA and D_2O. This consideration can be illustrated by Figure 5b, where the spectrum corresponding

to a low protein concentration (1.7 mM/L) does not exhibit the band around 210 cm^{-1}, previously identified as the signature of the coupling of protein and solvent dynamics.

Addition of trehalose mainly induces the limitation of the distribution of the side chains vibrations at the water−protein interface. Consequently, the transformation of the $\Delta\chi''(\nu)$ spectrum above 200 cm^{-1} by addition of trehalose (Figure 6b) can be interpreted as the reduction of the dynamic fluctuations at the protein−water interface in relation with the strengthening of the intermolecular O−H interactions in water. This is consistent with the great ability of trehalose to form H-bonds with water, and to distort the H-bond network of water.[18,33] Molecular associations between trehalose and water could be responsible for the reduction of SASA observed by addition of trehalose at room temperature (Figure 3) and keeping water hydration around the protein in the denatured state observed in Figure 7b. This can explain why trehalose stabilizes the tertiary structure of proteins, and thus explain the protein thermostabilization mechanism. These interpretations are consistent with the preferential hydration hypothesis.[5,15,34] The influence of trehalose on BSA and LYS dynamics analyzed in the present study is in agreement with recent quasi-elastic neutron scattering investigations on C-phycocianin.[35]

Acknowledgment. This work is supported by Agence Nationale de la Recherche (program Physique Chimie du Vivant).

References and Notes

(1) Crowe, L. M.; Reid, D. S.; Crowe, J. H. *Biophys. J.* **1996**, *71* (4), 2087. Fox, K. C. *Science* **1995**, *267* (5206), 1922.

(2) Hédoux, A.; Willart, J. F.; Ionov, R.; Affouard, F.; Guinet, Y.; Paccou, L.; Lerbret, A.; Descamps, M. *J. Phys. Chem. B* **2006**, *110*, 22886.

(3) Cottone, G.; Giuffrida, S.; Ciccotti, G.; Cordone, L. *Proteins* **2005**, *59* (2), 291.

(4) Crowe, J. H.; Crowe, L. M.; Oliver, A. E.; Tsvetkova, N.; Wolkers, W.; Tablin, F. *Cryobiology* **2001**, *43* (2), 89. Crowe, L. M.; Mouradian, R.; Crowe, J. H.; Jackson, S. A.; Womersley, C. *Biochim. Biophys. Acta* **1984**, *769* (1), 141.

(5) Timasheff, S. N. *Proc. Natl. Acad. Sci. U.S.A.* **2002**, *99* (15), 9721.

(6) Green, J. L.; Angell, C. A. *J. Phys. Chem.* **1989**, *93*, 2880.

(7) Branca, C.; Magazu, S.; Maisano, G.; Migliardo, P. *J. Chem. Phys.* **1999**, *111* (1), 281.

(8) Hédoux, A.; Ionov, R.; Willart, J. F.; Lerbret, A.; Affouard, F.; Guinet, Y.; Descamps, M.; Prevost, D.; Paccou, L.; Danède, F. *J. Chem. Phys.* **2006**, *124*, 14703.

(9) Hedoux, A.; Affouard, F.; Descamps, M.; Guinet, Y.; Paccou, L. *J. Phys.: Condens. Matter* **2007**, *19* (20), 8.

(10) Williams, R. W.; Dunker, A. K. *J.Mol. Biol.* **1981**, *152* (4), 783. Levitt, M.; Greer, J. *J. Mol. Biol.* **1977**, *114* (2), 181.

(11) Vaney, M. C.; Maignan, S.; Ries-Kautt, M.; Ducriux, A. *Acta Crystallogr., Sect. D, Biol. Crystallogr.* **1996**, *52* (Part 3), 505.

(12) Lerbret, A.; Bordat, P.; Affouard, F.; Hedoux, A.; Guinet, Y.; Descamps, M. *J. Phys. Chem. B* **2007**, *111*, 9410.

(13) Kabsch, W.; Sander, C. *Biopolymers* **1983**, *22* (12), 2577.

(14) He, X. M.; Carter, D. C. *Nature (London)* **1992**, *358* (6383), 209.

(15) Timasheff, S. N. *Biochemistry* **2002**, *41* (46), 13473.

(16) Militello, V.; Casarino, C.; Emanuele, A.; Giostra, A.; Pullara, F.; Leone, M. *Biophys. Chem.* **2004**, *107* (2), 175.

(17) Bordat, P.; Lerbret, A.; Demaret, J. P.; Affouard, F.; Descamps, M. *Europhys. Lett.* **2004**, *65* (1), 41. Lerbret, A.; Bordat, P.; Affouard, F.; Descamps, M.; Migliardo, F. *J. Phys. Chem. B* **2005**, *109*, 11046.

(18) Lerbret, A.; Bordat, P.; Affouard, F.; Guinet, Y.; Hedoux, A.; Paccou, L.; Prevost, D.; Descamps, M. *Carbohydr. Res.* **2005**, *340* (5), 881.

(19) Michnik, A.; Michalik, K.; Drzaga, Z. *J. Therm. Anal. Calorim.* **2005**, *80*, 399.

(20) Ross, P. D.; Shrake, A. *J. Biol. Chem.* **1988**, *263* (23), 11196.

(21) Efimova, Y. M.; Haemers, S.; Wierczinski, B.; Norde, W.; van-Well, A. A. *Biopolymers* **2007**, *85* (3), 264.

(22) Surewicz, W. K.; Mantsch, H. H.; Chapman, D. *Biochemistry* **1993**, *32*, 389.

(23) van-Stokkum, I. H.; Linsdell, H.; Hadden, J. M.; Haris, P. I.; Chapman, D.; Bloemendal, M. *Biochemistry* **1995**, *34*, 10508.

(24) Caliskan, G.; Mechtani, D.; Roh, J. H.; Kisliuk, A.; Sokolov, A. P.; Azzam, S.; Cicerone, M. T.; Lin Gibson, S.; Peral, I. *J. Chem. Phys.* **2004**, *121* (4), 1978. Leslie, S. B.; Israeli, E.; Lighthart, B.; Crowe, J. H.; Crowe, L. M. *Appl. Environ. Microbiol.* **1995**, *61* (10), 3592.

(25) Kaushik, J. K.; Bhat, R. *J. Biol. Chem.* **2003**, *278* (29), 26458.

(26) Idrissi, A.; Longelin, S.; Sokolic, F. *J. Phys. Chem. B* **2001**, *105*, 6004. Nakayama, T. *Phys. Rev. Lett.* **1998**, *80* (6), 1244. Padro, J. A.; Marti, J. *J. Chem. Phys.* **2003**, *118* (1), 452.

(27) Giraud, G.; Karolin, J.; Wynne, K. *Biophys. J.* **2003**, *85* (3), 1903.

(28) Colaianni, S. E. M.; Nielson, O. F. *J. Mol. Struct.* **1995**, *347*, 267.

(29) Giraud, G.; Wynne, K. *J. Chem. Phys.* **2003**, *119* (22), 11753.

(30) Dirama, T. E.; Curtis, J. E.; Carri, G. A.; Sokolov, A. P. *J. Chem. Phys.* **2006**, *124* (3), 034901.

(31) Bleustein, C. B.; Sennett, M.; Kung, R. T.; Felsen, D.; Poppas, D. P.; Stewart, R. B. *Lasers Surgery Med.* **2000**, *27* (5), 465.

(32) Salvetti, G.; Tombari, E.; Mikheeva, L.; Johari, G. P. *J. Phys. Chem. B* **2002**, *106*, 6081.

(33) Branca, C.; Magazu, S.; Maisano, G.; Migliardo, P.; Villari, V.; Sokolov, A. P. *J. Phys. Condens. Matter* **1999**, *11* (19), 3823.

(34) Xie, G.; Timasheff, S. N. *Biophys. Chem.* **1997**, *64* (1−3), 25.

(35) Koper, I.; Combet, S.; Petry, W.; Bellissent-Funel, M. C. *Eur. Biophys. J.* **2008**, *37* (6), 739.

JP900330R